

Benchmark control problem for real-time hybrid simulation

Christian E. Silva^{a,*}, Daniel Gomez^{b,c}, Amin Maghareh^b, Shirley J. Dyke^a, and Billie F. Spencer Jr.^d

^a*School of Mechanical Engineering, Purdue University, West Lafayette, IN, 47906, U.S.A.*

^b*Lyles School of Civil Engineering, Purdue University, West Lafayette, IN, 47906 U.S.A.*

^c*School of Civil Engineering and Geomatics, Universidad del Valle, Cali, Colombia.*

^d*Department of Civil and Environmental Engineering, University of Illinois at Urbana-Champaign, Urbana, IL, 61801, U.S.A.*

Abstract

This paper presents the problem definition and guidelines for a benchmark control problem in real-time hybrid simulation for a seismically excited building. Benchmark problems have been especially useful in enabling a community of researchers to leap forward on a given topic, distill the lessons learned, and identify the capabilities and limitations of various approaches. The focus here is on the design of an effective transfer system displacement tracking controller which is a commonly used approach for ensuring that interface conditions between numerical and experimental substructures are satisfied. In this study, a laboratory model of a three-story steel frame is considered as the reference structure. Realistic numerical models are developed and provided to represent the numerical and experimental substructures and the transfer system, which is comprised of hydraulic actuation, sensing instrumentation, and control implementation hardware. Experimental components are identified and provided as Simulink models, which are executed in real-time using Simulink's Desktop Real-Time capability to enable realistic virtual real-time hybrid simulation. The task of each participant is to design, evaluate, and report on their proposed controller approaches using the numerical models and computational codes provided. Such approaches will be assessed for robustness and performance using the provided tools. This benchmark problem is expected to further the understanding of the relative merits, as well as provide a clear basis for evaluating the performance of various control approaches and algorithms for RTHS. To illustrate some of the design challenges, a sample control strategy employing a proportional-integral (PI) controller in addition to the built-in transfer system's own control loop is included.

*Corresponding author tel.: +1 (765) 494-6900

Email address: silva15@purdue.edu (Christian E. Silva)

Keywords: RTHS, Actuator Control, Structural Dynamics

1. Introduction

Despite past efforts to establish computational models of complex structural systems subjected to extreme loading conditions, simulation alone is often insufficient to understand these systems. Experimental testing is essential, and when the system under consideration is too large to fit in a laboratory, more creative testing methods need to be exploited. Hybrid simulation methods provide a critical bridge between physical experimentation and new developments in computational modeling [1, 2, 3, 4, 5, 6, 7, 8, 9, 10, 11, 12, 13, 14]. Additionally, hybrid simulation has the potential of providing essential capabilities to verify unproven innovations before they are brought to practice, such as new materials or novel design concepts which must be examined and validated experimentally [15].

Several classes of hybrid simulation methods have been explored in the past, each with its own significant and unique challenges and capabilities. Traditional hybrid simulation is conducted at an extended time scale, typically uses computational models with large number of degrees of freedom (DOF) and is applied when rate-dependence is not significant in the experimental subsystem [16, 17]. Real-time hybrid simulation (RTHS) is needed when rate-dependence plays a significant role in the dynamics of the experimental subsystem, although it requires both high-fidelity control of the actuation system and real-time execution of the numerical model and associated supervisory tasks [7, 18]. Furthermore, geographically-distributed hybrid simulation and geographically-distributed RTHS have been demonstrated in isolated cases to further expand the range of possible experiments by coupling multiple laboratories with different or supplemental resources, in terms of experimental equipment or computational capabilities. [19, 20, 21, 22, 23, 24].

Real-time hybrid simulation is a versatile experimental technique for examining structural behavior and validating performance [25, 26, 27, 28, 29, 30, 31, 32, 33]. This coupling of an experimental subsystem with a numerically modeled subsystem, according to a selected partitioning scheme, enables a detailed examination of the entire system while imposing realistic conditions at the boundary between the two subsystems. Such boundary conditions provide the reactions and interactions between the two adjacent substructures. RTHS is mainly used either when a structural system is too large or complex to evaluate using traditional techniques (e.g., high-rise buildings or long-span bridges), or when the response of a physical specimen cannot be predicted using the latest computational

models and its behavior must be observed under realistic operational conditions [17, 7, 34, 35, 36, 37, 33].

In the 2010s, advances in hybrid simulation methods have been the focus of several workshops around the world [38, 39, 40, 41, 42]. Moreover, a survey was 40 conducted in 2014 in the United States by the George E. Brown, Jr. Center for Network of Earthquake Engineering Simulation (NEES) Program, with support from the U.S. National Science Foundation. The purpose of this survey was to understand the barriers to using these techniques, and a NEES Task Force was charged with the writing of a primer intended for researchers new to hybrid simulation 45 [43]. In addition, the National Science Foundation has funded a research coordination network on this topic, called the Multi-hazard Engineering Collaboratory on Hybrid Simulation (MECHS). MECHS is intended to enable the body of researchers to make the advances needed for both establishing the fundamental theory and expanding the capacities of hybrid simulation methods for natural 50 hazards applications [42].

Benchmark problems have been especially useful in enabling a community of researchers to jump forward on a given topic, distill the lessons learned, and identify the capabilities and limitations of various methods. Beginning in 1996, the structural control community developed a series of benchmark problems on 55 buildings and bridges which considered both seismic and wind loading [44, 45, 46, 47, 48, 49, 50, 51, 52, 53, 54, 55, 56, 57, 58, 59]. This series of benchmark problems was instrumental in building awareness and overcoming several of the realistic challenges associated with structural control methods.

A benchmark problem in RTHS is proposed in this paper to stimulate advances 60 in this field and to broaden the base of users of these methods. The motivation for developing this benchmark problem is twofold: 1) to propose a realistic actuator tracking control problem for its application in RTHS in such a way that the community could explore a variety of solution methodologies and further advance the field; 2) to provide a computational framework in which RTHS experiments 65 with increasing levels of complexity can be performed virtually. Realistic models of the hydraulic components and physical control constraints are included within this RTHS framework. Participants are supplied with the framework, models, and computational codes based on an actual RTHS experiment available in the Intelligent Infrastructure Systems Laboratory (IISL) at Purdue University.

Participants should design suitable controllers, execute the virtual RTHS, and 70 report on both the performance and robustness of their design. To illustrate this approach, an example proportional-integral (PI) controller is provided. With these realistic models and the flexible framework included here, we anticipate that the

models, framework, and codes provided will also be useful for launching a variety
75 of additional studies, and participants are encouraged to consider such opportunities. It should be mentioned that the provided materials and codes were prepared in MATLAB R2014a [60].

2. Reference model of the benchmark control problem

This section provides the description of the physical structure followed by
80 the development of the reference model for the benchmark problem. Subsections 2.1, 2.2, and 2.3 explain the models used, and Subsection 2.4 provides an explanation of how partitioning is performed.

2.1. Physical structure

The benchmark problem considers a laboratory model of a typical three-story
85 steel frame structure, used in past RTHS experiments in the IISL. The structure considered for this study was partly designed and built by Gao [61] as part of an effort to develop a comprehensive and robust framework for RTHS that would include the experimental setup, computational hardware, computational codes, and a set of experiments with different levels of complexity [62, 63, 18].

90 The geometry and dimensions of the three-story, two-bay physical structure are shown in Fig. 1. The floors of the structure are numbered with respect to the ground level, with the 3rd floor being the roof. Base supports are designed as pinned connections which provide a structure with zero moment, minimizing the formation of plastic hinges at the base during testing. The columns are made from
95 commercial S3 × 5.7 sections. The custom beam elements are welded assemblies using 50 × 6 mm webs and 38 × 6 mm flanges. Both the columns and beams of this system are made from structural steel.

A strong-column weak-beam design concept is implemented on the physical structure, instead of a shear frame assumption which would commonly be chosen
100 for this type of problem. The final assembly has an aspect ratio of 1.75, providing a dynamic behavior and properties similar to those of large-scale frames. The beams and columns are connected through moment-resisting bolted connections with high strength steel bolts and lock nuts.

2.2. Finite element model

105 Based on the physical characteristics of the structure, a planar finite element (FE) model is constructed assuming moment-resisting behavior in the frame. The FE model considers the contributions of all structural elements, and their different

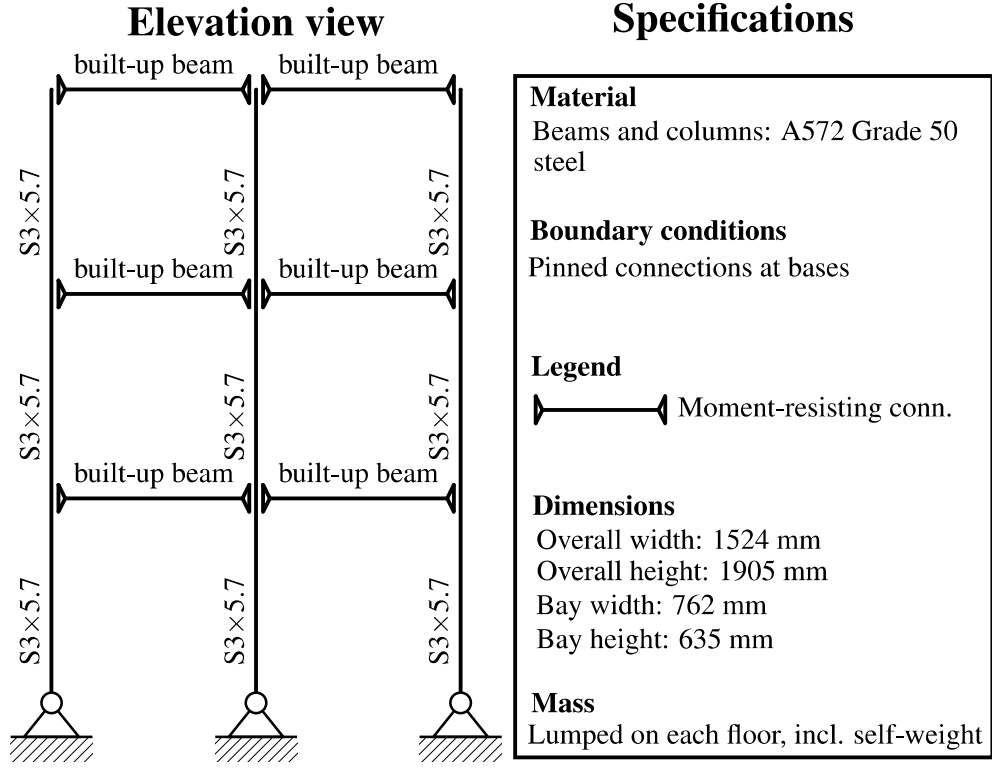


Figure 1: Benchmark structure details and specifications.

modes of deformation (axial, shear, and bending) on the calculation of the equations of motion. Beams and columns are modeled with 2D beam-column finite elements to form the global mass and stiffness matrices. The material properties are considered to be homogeneous for all elements, with linear elastic behavior. A discretization scheme using one node per beam-column connection is used, with each node having 3-DOF including horizontal and vertical translations, as well as rotation around the normal direction. Proportional damping is assumed. The total number of DOF initially in the FE model is 30-DOF, including the three rotations of the boundary conditions, as shown in Fig. 2, left.

2.3. Reference model

Next, several assumptions are made to reduce the order of the FE model without loss of relevant and necessary information. This step is helpful because the FE model has a large number of DOF and high frequency dynamics (effects of rotational DOF with relatively small inertia) that could hinder the stability of the

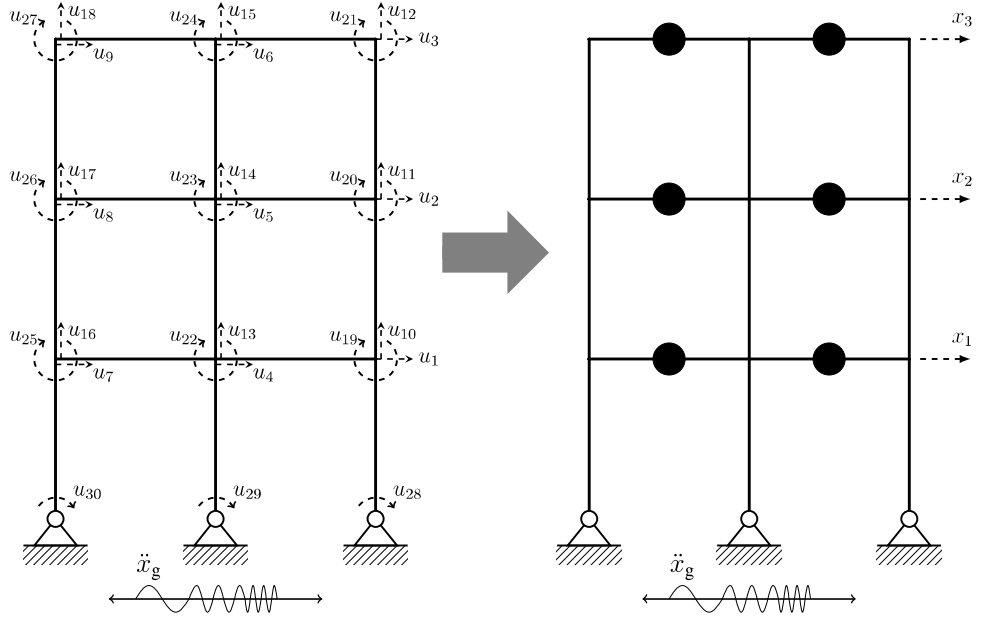


Figure 2: FE model (left) and reference model (right).

RTHS and, to some extent, complicate the partitioning process. Specifically, these assumptions include: (1) the vertical translations of all the nodes of the model are neglected as axially stiff columns are assumed, which reduces the model to 21-DOF; (2) the horizontal relative displacements between nodes of the same floor are very small (i.e., a rigid diaphragm assumption), which reduces the model to 15-DOF; thus, (3) lumped masses are assumed at the middle of each span, based upon their tributary areas (see Fig. 2, right); and, (4) static condensation is applied by apportioning the mass and stiffness matrices into dynamic (non-zero mass) and zero mass DOF. Once this step is completed, the transformation matrix is determined, and the condensed mass, stiffness and input terms of the equations of motion are obtained [64]. These series of operations altogether reduce the model to 3-DOF. These assumptions were confirmed by comparing the horizontal displacements obtained from the finite element and reference model. The equation of motion (EOM) for the resulting model, which will hereafter be referred to as the *reference model*, is given by

$$\mathbf{M}_r \ddot{\mathbf{x}} + \mathbf{C}_r \dot{\mathbf{x}} + \mathbf{K}_r \mathbf{x} = -\mathbf{M}_r \ddot{x}_g, \quad (1)$$

where \mathbf{M}_r , \mathbf{C}_r , and \mathbf{K}_r are the mass, stiffness and damping matrices of the reference model, respectively, \mathbf{x} , $\dot{\mathbf{x}}$, and $\ddot{\mathbf{x}}$ are the displacement, velocity and acceleration vectors, and \ddot{x}_g is the ground motion input.

tion vectors, respectively, all relative to the ground, \ddot{x}_g is the ground acceleration and τ is the influence coefficient vector, which contains a value of one for each mass that develops an inertial force when the whole system is accelerated horizontally. Overdots indicate a derivative with respect to time. Using modal damping ratios, the damping matrix of the reference structure is given by

$$\mathbf{C}_r = (\Phi^\top)^{-1} \hat{\mathbf{C}}_r \Phi^{-1}, \quad (2)$$

where Φ is the modal matrix and the $(\cdot)^\top$ symbol denotes the transpose operation. In this equation, $\hat{\mathbf{C}}_r$ is

$$\Phi^\top \mathbf{C}_r \Phi = \hat{\mathbf{C}}_r = \begin{bmatrix} 2\zeta_1 \omega_1 m_1 & & \\ & 2\zeta_2 \omega_2 m_2 & \\ & & 2\zeta_3 \omega_3 m_3 \end{bmatrix}, \quad (3)$$

where ζ_i is the modal damping ratio, ω_i is the natural frequency related to the i -th mode of vibration, and m_i is the generalized modal mass of the i -th floor of the reference model. Note that in the four case studies that will be defined in subsequent sections, the modal damping ratios for the reference model will be varied.

2.4. Partitioned Equations of Motion

For RTHS, the reference model must be partitioned into numerical and experimental substructures. The mass and stiffness matrices of the reference structure are considered as a sum of the corresponding matrices of the numerical and experimental substructures, given by

$$\begin{aligned} \mathbf{M}_r &= \mathbf{M}_e + \mathbf{M}_n \\ \mathbf{K}_r &= \mathbf{K}_e + \mathbf{K}_n \\ \mathbf{C}_r &= \mathbf{C}_e + \mathbf{C}_n, \end{aligned} \quad (4)$$

where the $(\cdot)_e$ and $(\cdot)_n$ subscripts refer to experimental and numerical, respectively, and $\mathbf{M}_e = \text{diag}(m_e, 0, 0)$, $\mathbf{C}_e = \text{diag}(c_e, 0, 0)$, and $\mathbf{K}_e = \text{diag}(k_e, 0, 0)$. Parameters m_e , c_e , k_e are the mass, stiffness and damping of the experimental substructure. The damping matrix of the numerical substructure is obtained from calculating the damping matrix of the reference model and then subtracting the identified damping matrix of the experimental substructure from it. This approach

is an approximation, although for low damping ratios is a reasonable assumption. Substituting Eqs. 4 into Eq. 1 and rearranging yields

$$\mathbf{M}_n \ddot{\mathbf{x}} + \mathbf{C}_n \dot{\mathbf{x}} + \mathbf{K}_n \mathbf{x} = -\mathbf{M}_r \ddot{\mathbf{x}}_g - \underbrace{(\mathbf{M}_e \ddot{\mathbf{x}} + \mathbf{C}_e \dot{\mathbf{x}} + \mathbf{K}_e \mathbf{x})}_{\mathbf{f}_e}, \quad (5)$$

where \mathbf{f}_e is the feedback force vector associated with the experimental substructure.

The partitioning process used for this benchmark problem is graphically represented in Fig. 3. The reference model is split into two substructures: numerical (dashed lines) and experimental (solid lines). The experimental substructure is the moment resisting frame available in the Intelligent Infrastructure Systems Lab (IISL) as described in Subsection 2.1, which is depicted in the zoomed-in portion of the figure. System identification techniques from experimental data are applied to the experimental substructure [61], to obtain the structural mass ($m_e = 29.1$ kg), lateral stiffness ($k_e = 1.19 \times 10^6$ N/m), and damping coefficient ($c_e = 114.6$ Nsec/m).

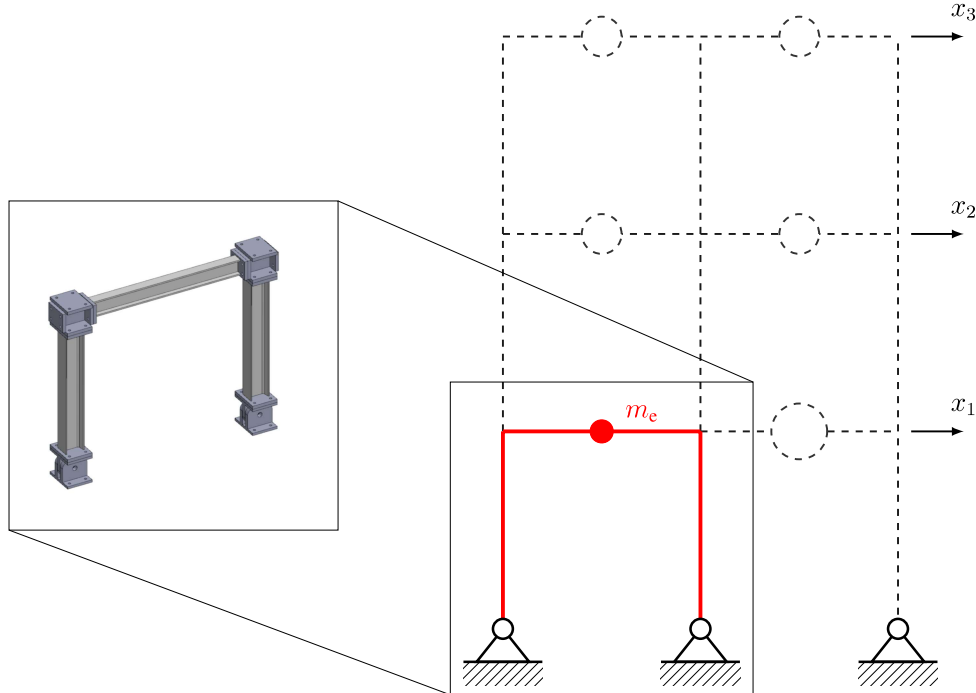


Figure 3: Numerical and experimental substructures.

The state-space representation of the numerical substructure is given by

$$\begin{bmatrix} \dot{\mathbf{z}}_n \\ \mathbf{y}_n \end{bmatrix} = \begin{bmatrix} \mathbf{A}_{ns} & | & \mathbf{B}_{ns} \\ \mathbf{C}_{ns} & | & \mathbf{D}_{ns} \end{bmatrix} \begin{bmatrix} \mathbf{z}_n \\ \mathbf{u}_n \end{bmatrix}, \quad (6)$$

135 where \mathbf{A}_{ns} is the state matrix, \mathbf{B}_{ns} the input matrix, \mathbf{C}_{ns} the output matrix, \mathbf{D}_{ns} the feedthrough matrix, \mathbf{z}_n the state vector given by $[\mathbf{x} \ \dot{\mathbf{x}}]^\top \in \mathbb{R}^6$, \mathbf{u}_n the input vector, given by $[\ddot{x}_g \ \mathbf{f}_e]^\top \in \mathbb{R}^4$ (\ddot{x}_g is the ground acceleration and \mathbf{f}_e is the feedback force vector), and \mathbf{y}_n the output vector given by $[\mathbf{x} \ \dot{\mathbf{x}} \ \ddot{\mathbf{x}}^\top]^\top \in \mathbb{R}^9$ (\mathbf{x} and $\dot{\mathbf{x}}$ are relative displacement and relative velocity vectors, and $\ddot{\mathbf{x}}^\top$ is the absolute or total acceleration vector). The state-space matrices in Eq. 6 are defined as

$$\begin{aligned} \mathbf{A}_{ns} &= \begin{bmatrix} \mathbf{0}_{3 \times 3} & \mathbf{I}_{3 \times 3} \\ -\mathbf{M}_n^{-1} \mathbf{K}_n & -\mathbf{M}_n^{-1} \mathbf{C}_n \end{bmatrix}_{6 \times 6} & \mathbf{B}_{ns} &= \begin{bmatrix} \mathbf{0}_{3 \times 1} & \mathbf{0}_{3 \times 3} \\ -\mathbf{M}_n^{-1} \mathbf{M}_r \mathbf{t} & -\mathbf{M}_n^{-1} \end{bmatrix}_{6 \times 4} \\ \mathbf{C}_{ns} &= \begin{bmatrix} \mathbf{I}_{3 \times 3} & \mathbf{0}_{3 \times 3} \\ \mathbf{0}_{3 \times 3} & \mathbf{I}_{3 \times 3} \\ -\mathbf{M}_n^{-1} \mathbf{K}_n & -\mathbf{M}_n^{-1} \mathbf{C}_n \end{bmatrix}_{9 \times 6} & \mathbf{D}_{ns} &= \begin{bmatrix} \mathbf{0}_{3 \times 1} & \mathbf{0}_{3 \times 3} \\ \mathbf{0}_{3 \times 1} & \mathbf{0}_{3 \times 3} \\ (-\mathbf{M}_n^{-1} \mathbf{M}_r + \mathbf{I}) \mathbf{t} & -\mathbf{M}_n^{-1} \end{bmatrix}_{9 \times 4}. \end{aligned} \quad (7)$$

3. Benchmark problem definition

This section is devoted to presenting the definition of the benchmark control problem for RTHS. Subsections 3.1 and 3.2 cover the partitioning of the structural system, and how this process is related to RTHS performance and stability.

145 In Subsection 3.3 the problem statement for the participants is presented and in Subsection 3.4 the evaluation criteria is explained. Finally, realistic implementation constraints and their relationship with the experimental setup available in the IISL are covered in Subsection 3.5.

3.1. Considerations due to partitioning

150 Test configuration (i.e., partitioning a reference structure into numerical and experimental substructures) plays a critical role in the successful implementation of an RTHS test [65, 66, 67, 68]. The interface between the numerical and experimental substructures is enforced through a mechanical device which will be referred to hereafter as the *transfer system*. The transfer system usually consists of a hydraulic actuator or shake table, which has inherent dynamics. These added dynamics are sensitive to the partitioning between numerical and experimental

substructures. Therefore, making appropriate decisions during the partitioning procedure is an important step towards a successful and stable RTHS experiment.

A control algorithm for the transfer system is required to accommodate the undesired dynamics at the interface. Without a proper controller, the dynamics of the transfer system may cause *de-synchronization* at the interface, including frequency-independent time-delay (caused by communication delay, A/D conversion, and computation delay), and frequency-dependent time-lag (caused by the transfer system inherent dynamics and control-structure interaction, CSI) leading to stability and performance issues. Horiuchi [69] expressed this stability problem for an SDOF system as an equivalent negative damping introduced to the experimental substructure. Moreover, these added dynamics in the feedback loop can result in instability or performance degradation [67].

In this study, the predictive stability indicator (PSI) is used to quantify the sensitivity of different partitioning choices to de-synchronization at the interface [67, 68]. The PSI is a pre-test design tool that provides a quantitative measure representing the sensitivity of the partitioning choice. In the PSI framework, a *virtual time-delay* (τ) is assumed at the interface (or feedback force) to quantitatively evaluate the sensitivity and minimum controller requirements of the partitioning choice (see Fig. 4). Thus, the partitioned equation of motion is presented as follows:

$$\mathbf{M}_n \ddot{\mathbf{x}} + \mathbf{C}_n \dot{\mathbf{x}} + \mathbf{K}_n \mathbf{x} = -\mathbf{M}_r \ddot{\mathbf{x}}_g - \mathbf{f}_e(t - \tau), \quad (8)$$

where τ is the virtual time-delay and \mathbf{f}_e is defined in Eq. 5. In the absence of the virtual time-delay ($\tau = 0$) the response of this system (Eq. 8), is identical to the response of the reference structure (Eq. 1). However, this is not realistic in the case of RTHS, as the interface conditions are enforced through the transfer system. The PSI is defined as $PSI = \log_{10}(\tau_{cr})$, where τ_{cr} is the critical time-delay (in msec), associated with the occurrence of a stability switch (change from a stable state to an unstable state) of the system in Fig. 4 at $\tau = \tau_{cr}$ [68].

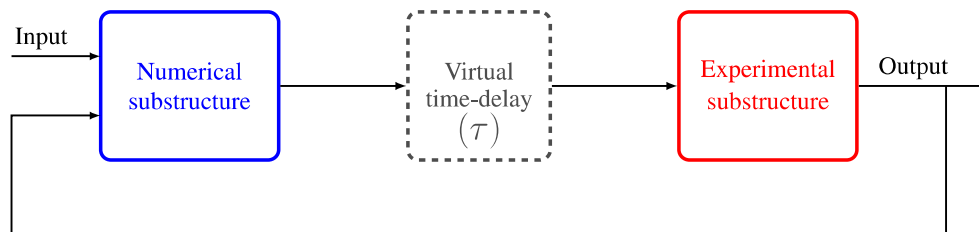


Figure 4: Predictive stability indicator framework.

3.2. Partitioning cases in the benchmark control problem

185 For this benchmark problem, four different partitioning cases are selected for participants to use for their control design and evaluation. These test cases serve for evaluating the robustness and performance of the proposed control approaches and the reason to have multiple cases is to provide a broad range of possible performance and stability behaviors of the system during the experiments.

190 Since a fixed experimental substructure is used, the partitioning cases are defined by varying the structural parameters of the reference structure, as shown in Table 1. Variations are considered in both the modal damping and the mass of each floor of the reference structure, thus yielding different stability and performance scenarios. For each case, the damping matrix is constructed using the same modal damping for all three modes, and the mass is the same for each floor. As mentioned earlier, the partitioning process consists of: 1) calculating the matrices M_r , C_r , and K_r using Table 1; 2) then subtract M_e , C_e , and K_e from M_r , C_r , and K_r , respectively to obtain M_n , C_n , and K_n according to Eq. 4.

195

Partitioning configuration	Reference floor mass (kg)	Reference modal damping (%)
Case 1	1000	5
Case 2	1100	4
Case 3	1300	3
Case 4	1000	3

Table 1: RTHS partitioning cases.

200 Results from previous experiences with the PSI show that the sensitivity of an experiment setup to de-synchronization, based on the chosen partitioning choice can be: 1) slightly sensitive, when the associated PSI is greater than 0.7, and the critical time-delay is greater than 5 msec; 2) moderately sensitive, when the associated PSI is between between 0 and 0.7, and the critical time-delay ranges from 1 msec to 5 msec; and, 3) extremely sensitive, when the associated PSI is less than 0, and the critical time-delay is less than 1 msec. These guidelines can be used to select a partitioning choice suited to the experience of the control designer. All of the cases selected for this problem statement have been chosen in such a way that their associated PSI lie either in the moderately or slightly sensitive regions (See Fig. 5).

205

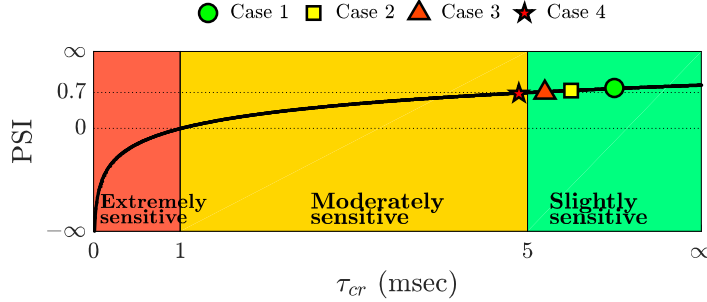


Figure 5: Sensitivity regions in the PSI vs. τ_{cr} diagram with the four cases of this study marked.

210 The PSI of the four partitioning cases are obtained from Fig. 6, where the
 topological lines represent different PSI values. The four cases of this study are
 represented with different markers in this plot. Even though only four cases are
 defined, participants are encouraged to go beyond these cases and explore other
 configurations, using this plot as a preliminary guideline for stability and perfor-
 mance. It should be mentioned that this paper explores the case of RTHS with
 215 1-DOF at the interface between substructures.

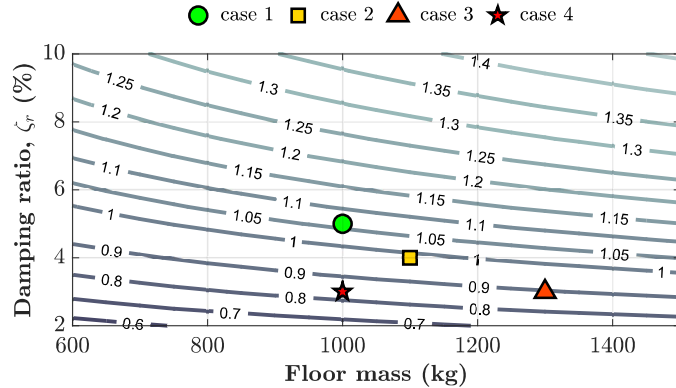


Figure 6: Predictive stability indicator for the defined partitioning cases, based on structural pa-
 rameters of the reference structure (m_e , c_e , and k_e are defined in Subsection 2.4). Topological lines
 represent PSI levels.

3.3. Control problem statement

A block diagram of the RTHS implementation for this benchmark problem is shown in Fig. 7. After the structure has been partitioned into numerical and experimental substructures and expressed in state-space form, the ground acceleration, \ddot{x}_g , and force feedback vector, \mathbf{f}_e , are input into the numerical substructure and its output vector, \mathbf{y}_n , is computed. In general, one or more elements of this vector may be used as the input to the controller. The command signal from the controller to the transfer system, y_{G_c} , is generated by the designed controller. The force at the first floor, f_e , measured in the experimental substructure, is fed back to the numerical substructure as vector \mathbf{f}_e , to execute the next numerical integration step. Vector \mathbf{f}_e can be expressed as

$$\mathbf{f}_e = \gamma f_e, \quad (9)$$

where γ is a column vector defined by the spatial location and direction of the interface DOF. For the configuration in this benchmark problem, $\gamma = [1 \ 0 \ 0]^\top$.

- 220 The measured force and displacement of the experimental substructure form the output vector, $\mathbf{y}_{G_p} = [f_e \ x_m]^\top$, whose elements can be used for feedback control. In this benchmark problem the complete system is executed in real-time on a target computer (denoted here as virtual RTHS, or vRTHS), and thus both the experimental substructure and transfer system are represented with numerical models.
- 225 It should be mentioned that all of the states of the numerical substructure are available in the model included with the companion computational codes.

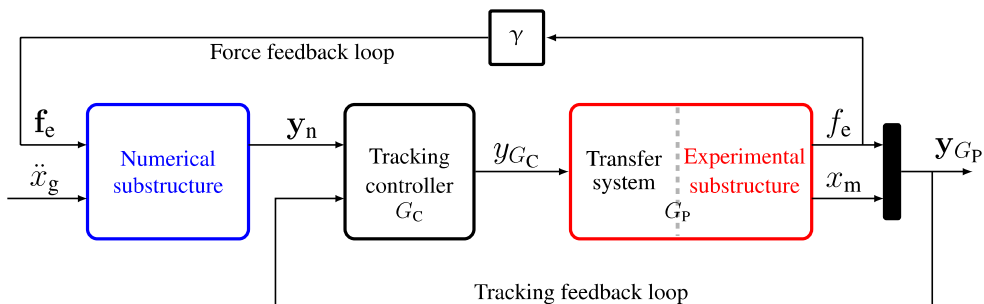


Figure 7: Block diagram of single-actuator RTHS.

- The integration is executed using an explicit fourth-order Runge-Kutta numerical integration scheme (ode4) with a fixed time step, selected for its simplicity and versatility in dynamic models built in Simulink. The Simulink model (included in the companion file package) serves as the execution tool for vRTHS,

and requires Simulink Desktop Real-time functionality of MATLAB [60]. Realistic constraints related to the execution time and control are defined herein to ensure that all controllers can be implemented within the vRTHS tool, and thus on the physical setup. The results should be presented based on vRTHS simulations.

235 A schematic of the physical elements (transfer system coupled with the experimental substructure) is shown in Fig. 8. In the physical setup, a linear fatigue-grade, double-ended servo-hydraulic actuator (Shore Western, 910D series) with a maximum rated force of 10.28 kN and a stroke of ± 63 mm, is used. The actuator is connected to the experimental substructure at the first floor. An embedded linear variable differential transformer (LVDT) transducer provides the displacement measurement of this actuator, and a fatigue-rated low-profile load cell (Interface, 1000 series) with a maximum rated force of 11.2 kN provides the force measurement of the structure. The hydraulic power supply is an MTS pump, with capacity of up to 680 l/min at 206 Bar.

240

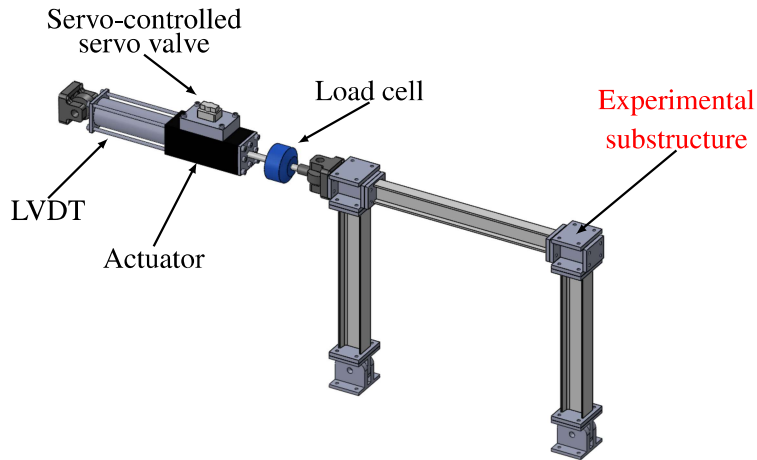


Figure 8: Control plant, consisting of the transfer system (servo-controlled actuator under unity-gain displacement feedback) coupled with the experimental substructure.

The plant to be controlled for tracking will be hereafter referred to as the *control plant*. This control plant includes the servo-controlled hydraulic actuator, the experimental substructure, and the sensing system consisting of the LVDT (displacement sensor) and load cell (force sensor). It should be mentioned that the sensing system is not included as a part of the Simulink model of the plant, but as a separate block outside from it. A schematic block diagram of this system is

shown in Fig. 9. The control plant is expressed in continuous state-space form as

$$\begin{aligned}\dot{\mathbf{z}}_{G_P} &= \mathbf{g}_1(\mathbf{z}_{G_P}, \mathbf{y}_{G_C}) \\ \mathbf{y}_{G_P} &= \mathbf{g}_2(\mathbf{z}_{G_P}, \mathbf{y}_{G_C}),\end{aligned}\quad (10)$$

245 where \mathbf{z}_{G_P} is the state vector of the control plant, \mathbf{y}_{G_P} is the output vector of the control plant specific for the design choice used in this study, and \mathbf{g}_1 and \mathbf{g}_2 are functional representations.

250 The task for the participants in this benchmark study is to define, evaluate and report on their proposed transfer system tracking control approaches. Using the models provided, participants will design and implement tracking controllers for this control plant, demonstrate their robustness to noise, uncertainties and modeling errors, and evaluate their performance. To illustrate the process and some of the challenges, a sample controller employing a proportional-integral (PI) strategy is discussed later and included in the companion file packet. It is expected that 255 researchers will initially use the nominal numerical model provided. However, the framework made available through this benchmark problem will readily allow participants to examine a broad range of problems by adjusting the partitioning, reference model and/or actuator parameters.

260 To achieve the desired response of the transfer system for RTHS execution, a tracking controller is required (see Fig. 9, where the feedback control system is shown highlighted). By modifying the contents of the tracking controller block in Simulink, participants can design controllers using various techniques, and then evaluate the performance of each controller designed.

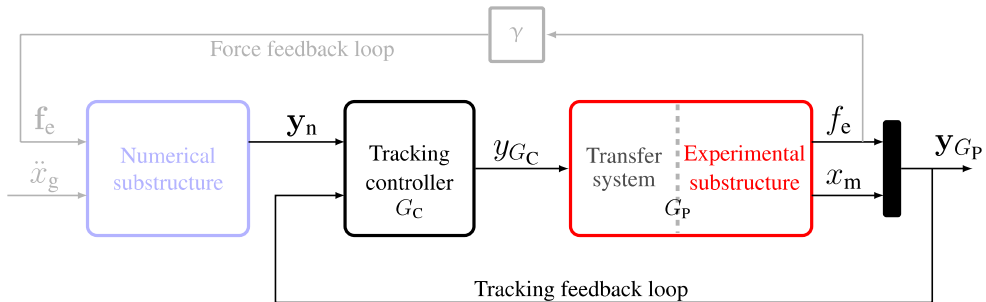


Figure 9: Feedback control system (highlighted).

The tracking controller, G_c should be implemented in discrete time and should take the form

$$\begin{aligned}\mathbf{z}_{G_C}[k+1] &= \mathbf{g}_3(\mathbf{z}_{G_C}[k], \mathbf{y}_n[k], \mathbf{y}_{G_P}[k]) \\ y_{G_C}[k] &= \mathbf{g}_4(\mathbf{z}_{G_C}[k], \mathbf{y}_n[k], \mathbf{y}_{G_P}[k]),\end{aligned}\quad (11)$$

265 where $\mathbf{z}_{G_C}[k + 1]$ is the controller state vector at time $t = (k + 1)\Delta T$, $y_{G_C}[k]$ is the controller output, at time $t = k\Delta T$ (k is the discrete index and ΔT is the simulation sampling duration), and g_3 and g_4 are functional representations.

270 In the sample control design to be discussed in Section 5, a single-input single-output (SISO) unity-gain proportional-integral feedback controller is used. Other types of compensator architectures may be implemented in this block. Just a few examples of alternate architectures for tracking control include the feedback-feedforward compensation introduced by [25], the adaptive time-series (ATS) compensator developed by [70], or the Robust Integrated Actuator Controller developed by [37].

3.4. Implementation constraints

275 The objective of participating in this benchmark problem is to design high performance controllers that can be implemented on the experimental system to perform RTHS. Thus, several implementation constraints are defined based on the physical devices available in the laboratory and are used in the Simulink codes.

1. The entire architecture of the controller has to be in discrete form.
- 280 2. The sampling frequency of the vRTHS test is 4096 Hz.
3. In each run of the vRTHS, the servo-hydraulic actuator responses cannot exceed the maximum capacity of the physical setup, including a maximum force of 8900 N, a stroke of ± 7 mm, and a maximum velocity of 300 mm/sec for this experiment.
- 285 4. The A/D and D/A converters are high accuracy analog I/O boards with 18 bit precision and a span of ± 3.8 V. These are modeled as a saturation block combined with a quantizer in the Simulink model.
5. The Simulink model considers the sensor conversion factors needed to form a voltage signal to the corresponding physical measurement. These parameters are: voltage to displacement in mm: 7.89 mm/V ; voltage to force in N: 1096 N/V.
- 290 6. Measurement noise statistics are obtained from experimental observations. Each measured response contains an RMS noise of 0.002 V, which is approximately 0.05 % of the full span of the A/D converter. The measurement noise is modeled as a Gaussian rectangular pulse process with a width of 0.2 msec.

7. The discrete-time controller can have any number of states (x_{G_C}). Also, it can use as many elements of the numerical substructure output vector (y_n), as well as the measurement vector (y_{G_P}) as needed, provided that the computations can be fully executed in a single time step.
8. The time-delay associated with a controller design should generally be less than 10 msec. Designers should aim for a time-delay value that, at a minimum, satisfies the critical time-delay of each case defined (Case 1 to Case 4).
9. Uncertainties must be considered in the evaluation to ensure that the controller is robust to unmodeled dynamics and model identification errors. Here such uncertainties are defined by varying the coefficients of the parametric model of the control plant (to be provided in Subsection 4.2). Each model with parameters different from the nominal ones will be referred to as a *perturbed model*. The companion codes and models have the capability to randomly generate perturbed models automatically each time the simulation is run. For realistic evaluation of the robust performance of each controller, at least 20 randomly generated runs for each partitioning case should be executed and documented. The perturbed models and parameter distributions will be discussed in Subsection 4.3

3.5. Evaluation criteria

To quantitatively evaluate the performance of each controller for RTHS, nine evaluation criteria are to be computed. The first three evaluation criteria consider the performance of the tracking controller. The remaining evaluation criteria consider the global performance of the RTHS, which is to be compared to the response of the reference model. Note that although the responses of the reference model would typically not be available for an RTHS, it is employed for this benchmark problem to support evaluation of the performance of various control strategies. Throughout the remaining of this paper, parenthesized superscripts represent vector elements.

The first evaluation criterion is the tracking time-delay. To determine the tracking time-delay, the cross correlation between desired and measured displacements is first calculated to estimate the time-delay. This value represents the integer number of simulation steps that the measured response must be shifted until a maximum correlation value is obtained. Determining the maximum correlation

corresponds to determining when the measured response aligns best with the command signal. When this integer is multiplied by the sampling frequency it determines the time-delay in milliseconds. J_1 is defined as

$$J_1 = \arg \max_k \left(\sum_i \mathbf{y}_n^{(1)}(i) x_m(i - k) \right). \quad (12)$$

The second evaluation criterion is the normalized root mean square (RMS) of the tracking error. This indicator, J_2 , represents the difference between the measured and desired displacement of the actuator [71] and is given by

$$J_2 = \sqrt{\frac{\sum_{i=1}^N [x_m(i) - \mathbf{y}_n^{(1)}(i)]^2}{\sum_{i=1}^N [\mathbf{y}_n^{(1)}(i)]^2}} \times 100\%, \quad (13)$$

where N is the number of data points.

The third evaluation criterion is the peak tracking error. This criterion, J_3 , computes the maximum value of the instantaneous error between the measured and desired actuator displacements, normalized by the maximum desired displacement [72],

$$J_3 = \frac{\max |x_m(i) - \mathbf{y}_n^{(1)}(i)|}{\max |\mathbf{y}_n^{(1)}(i)|} \times 100\%. \quad (14)$$

The fourth criterion is the normalized RMS global displacement error which evaluates the difference between the reference and the measured response at the DOF of interest. For the first floor in this benchmark problem this is computed based on the measurement at the interface between the numerical and experimental substructures [72]. However, for the upper floors the response of the numerical substructure must be used,

$$J_4 = \sqrt{\frac{\sum_{i=1}^N [x_m(i) - \mathbf{x}_r^{(1)}(i)]^2}{\sum_{i=1}^N [\mathbf{x}_r^{(1)}(i)]^2}} \times 100, \quad (15)$$

where \mathbf{x}_r is the vector of displacements in the reference structure. The fifth criterion is the normalized RMS relative displacement of the second floor, evaluated

using from the RTHS and the reference responses,

$$J_5 = \sqrt{\frac{\sum_{i=1}^N [\mathbf{y}_n^{(2)}(i) - \mathbf{x}_r^{(2)}(i)]^2}{\sum_{i=1}^N [\mathbf{x}_r^{(2)}(i)]^2}} \times 100\%. \quad (16)$$

The sixth criterion is the normalized RMS relative displacement of the third floor. Again, the numerical response is considered instead of the measured response as the latter is not available,

$$J_6 = \sqrt{\frac{\sum_{i=1}^N [\mathbf{y}_r^{(3)}(i) - \mathbf{x}_r^{(3)}(i)]^2}{\sum_{i=1}^N [\mathbf{x}_r^{(3)}(i)]^2}} \times 100\%. \quad (17)$$

The seventh criterion is the peak global displacement error. This is similar to the peak tracking error, but the displacement of the first floor of the reference model is compared with the measured response [72],

$$J_7 = \frac{\max |x_m(i) - \mathbf{x}_r^{(1)}(i)|}{\max |\mathbf{x}_r^{(1)}(i)|} \times 100\%. \quad (18)$$

The eight criterion is the peak relative displacement error corresponding to the second floor. For this case, the numerical response of the second floor is compared with its counterpart in the reference response,

$$J_8 = \frac{\max |\mathbf{y}_n^{(2)}(i) - \mathbf{x}_r^{(2)}(i)|}{\max |\mathbf{x}_r^{(2)}(i)|} \times 100\%. \quad (19)$$

The final ninth criterion corresponds to the peak relative displacement error corresponding to the third floor,

$$J_9 = \frac{\max |\mathbf{y}_n^{(3)}(i) - \mathbf{x}_r^{(3)}(i)|}{\max |\mathbf{x}_r^{(3)}(i)|} \times 100\%. \quad (20)$$

4. Virtual RTHS (vRTHS)

In this section, a general explanation of the vRTHS tool is provided for evaluation of the participant control designs. Subsection 4.1 provides an overview of the vRTHS tool and the relationship between different Simulink blocks with the RTHS model, which are explained in Subsection 4.2. Subsection 4.3 discusses the parametric uncertainties in the control plant. The computational codes, models and data included in the companion code package are listed in Subsection 4.4. The expected deliverables from participants are discussed in Subsection 4.5.

335 *4.1. General overview*

The vRTHS tool is implemented using computational code developed in MATLAB and Simulink RT 2014 [60], which are included in the companion file package. A general schematic diagram of the implementation is shown in Fig. 10. A `Readme.pdf` file is also included in the companion code package with further explanation of the codes and how to get started.

340 Execution takes place in the MATLAB environment. To generate the sub-structure models, the algorithm loads the controller, and initializes the parameters of the simulation in `Run_vRTHS_MDOF.m`. This script calls the Simulink model `vRTHS_MDOF_SimRT2014a.slx` which executes the virtual RTHS. After the simulation, and once the results are obtained, the main script computes the evaluation criteria and creates comparison plots. All these processes run sequentially from the same main script, `Run_vRTHS_MDOF.m`. The participant defines two main aspects of the problem, including the partitioning choice and the controller implementation.

350 *4.2. Transfer system model*

The control plant consists of the transfer system and the experimental sub-structure. For the development of this benchmark problem, a model of both components is identified to enable realistic vRTHS (see Section 2 for the experimental substructure parameters). The model of the transfer system is provided in a sub-355 system block in the Simulink model, with three blocks that include servo-valve dynamics, actuator dynamics and control-structure interaction (CSI). When coupled with the experimental substructure model they form the control plant, which should be used for control design.

The model of the transfer system is identified using a new method intended 360 for servo-hydraulic actuators that is similar to the method described in [73]. In this approach the transfer system is modeled using parametric expressions with

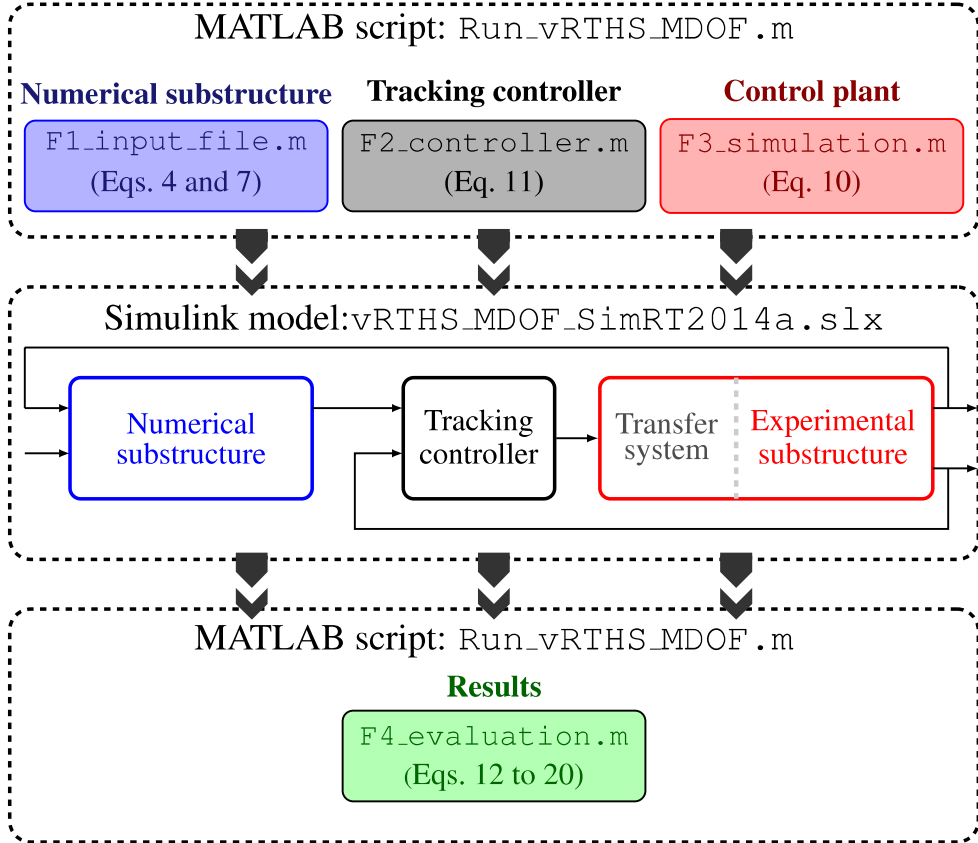


Figure 10: Flow diagram of the vRTHS computational tool, indicating the relationship between the codes and equations presented in this paper.

parameters that represent lumped physical constants in the servo-valve, hydraulic actuator and inner loop controller. This new modeling capability allows to separate the transfer system from the experimental substructure in the identification process, thus generating two models that can be modified to explore uncertainties or to vary the experimental setup. However, the CSI is fully accounted for in each of the models [74].

The control plant model is schematically represented in Fig. 11. The individual dynamics of the servo-valve, actuator, experimental substructure, and effects of CSI are modeled with appropriate transfer functions, with the signal quantities clearly marked and previously defined (Q is the flow-rate in the actuator). The dynamics of the servo-valve are modeled as a second-order linear system [75] with parameters $a_1\beta_0$, β_1 and β_2 .

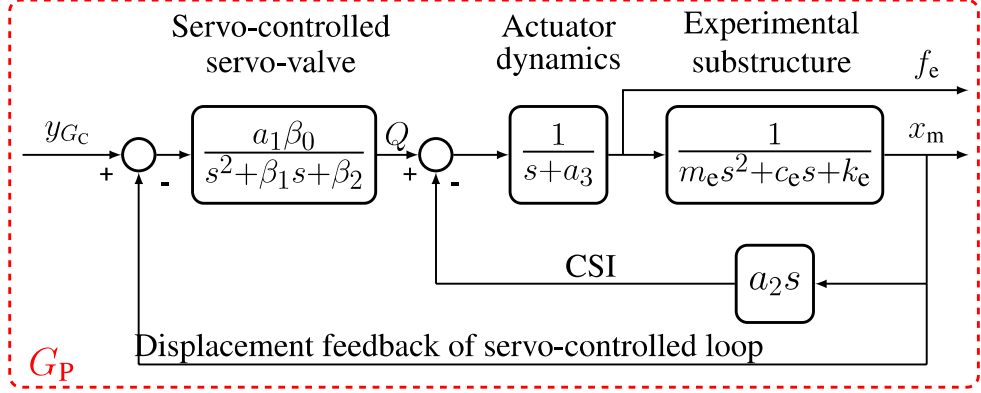


Figure 11: Block diagram of the control plant.

Similarly, the hydraulic actuator is represented as a first-order transfer function with the parameter a_3 , and the natural velocity feedback loop that results in CSI, with the parameter a_2 . The lumped parameters $a_1\beta_0$, β_1 , β_2 , a_2 and a_3 capture the physical characteristics of a full servo-hydraulic model in a more compact form, and their units and identified values are listed in Table 2. The plant has a closed-loop response obtained from the parametric systems of Fig. 11, by combining the corresponding transfer function blocks into a single system given by

$$G_P(s) = \frac{B_0}{A_5s^5 + A_4s^4 + A_3s^3 + A_2s^2 + A_1s + A_0}, \quad (21)$$

where

$$\begin{aligned} B_0 &= a_1\beta_0 \\ A_0 &= k_e a_3 \beta_2 + a_1\beta_0 \\ A_1 &= k_e a_3 \beta_1 + (k_e + c_e a_3 + a_2)\beta_2 \\ A_2 &= k_e a_3 + (k_e + c_e a_3 + a_2)\beta_1 + (c_e + m_e a_3)\beta_2 \\ A_3 &= (k_e + c_e a_3 + a_2) + (c_e + m_e a_3)\beta_1 + m_e \beta_2 \\ A_4 &= c_e + m_e a_3 + m_e \beta_1 \\ A_5 &= m_e. \end{aligned} \quad (22)$$

The identified numerical values of the parameters are provided in Table 2.

³⁷⁵ 4.3. Parametric uncertainties

This benchmark control problem accounts for model uncertainties that are included to ensure robust stability and robust performance in the resulting control

designs. Each participant should evaluate and discuss the robustness of their design by running a series of simulations that consider the performance of their controller when implemented on a system with parameters that are slightly different than those it is designed for, referred to here as the perturbed model. To generate random parameter variations, a region defining the uncertainty is constructed using a series of experiments. By disassembling and reassembling the experiment several times, several samples of the control plant transfer function are identified under similar conditions. From these models a region of uncertainty is constructed to define the range of responses of the control plant in the frequency domain. Variations in four parameters of the plant capture this region of uncertainty: the two parameters in the transfer function of the servo-valve that are associated with its time constant (β_1 and β_2), the parameter in the transfer function of the actuator that is associated with its time constant (a_3), and the stiffness of the experimental substructure (k_e). Each parameter is modeled as a random variable with a normal distribution. Table 2 also includes the mean and standard deviation of these parameters.

Parameter	Component	Nominal value (μ)	Std. dev. (σ)	Units
$a_1\beta_0$	Servo-valve	2.13×10^{13}	-	m Pa/sec
a_2	Actuator	4.23×10^6	-	m Pa
a_3	Actuator	3.3	1.3	1/sec
β_1	Servo-valve	425	3.3	unitless
β_2	Servo-valve	10×10^4	3.31×10^3	1/sec
m_e	Exp. sub.	29.1	-	kg
k_e	Exp. sub.	1.19×10^6	5×10^4	N/m
c_e	Exp. sub.	114.6	-	kg/sec

Table 2: Parametric values of the control plant.

The family of control plant transfer functions generated by modifying the model parameters is shown in Fig. 12. After a given control design is tested on the nominal (unperturbed) system, at least 20 simulations should be performed with different randomly generated models to demonstrate robust stability. These four parameters are randomly selected to generate perturbed models on which to run a given controller. The companion code package facilitates this process.

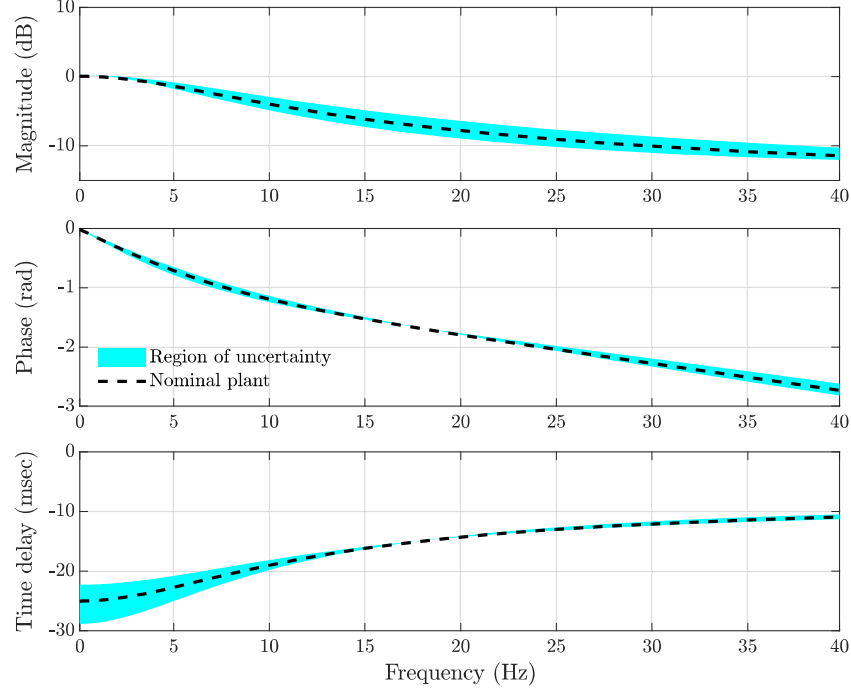


Figure 12: Frequency response regions of the perturbed-systems. The transfer function of the identified plant is shown in dashed lines.

⁴⁰⁰ 4.4. *Provided materials*

The materials provided in the companion codes include:

1. Models
 - (a) Reference model: a 3-DOF structural model (matrices M_r , C_r , and K_r , as described in Eq. 1).
 - (b) Experimental substructure: identified dynamic parameters m_e , c_e , and k_e (see Subsection 2.4).
 - (c) Transfer system: the parametric models of the servo-valve, hydraulic actuator and CSI (see Subsection 4.2).
2. Partitioning choices: the four cases defined in Table 1, and explained in Subsection 3.1.
3. Ground motion data: a set of three unscaled historic ground acceleration records: El Centro 1940, Kobe 2005 and Morgan Hill 1984, plus a chirp

415

block for verification purposes. These provide different RTHS experiment options, but this paper presents results only corresponding to El Centro earthquake.

420

4. Sample tracking controller: a sample controller in state-space form, based on a PI strategy with an additional phase lead pre-compensation block. The sample control design code is included in the companion files.
5. Virtual RTHS tool: a combined MATLAB/Simulink set of codes, scripts and data sets for running vRTHS for different control strategies and partitioning choices. A detailed explanation of these codes is included in the companion file package.

4.5. Expected deliverables

The expected deliverables from the participants of this benchmark problem definition are

425

430

435

440

1. Tracking controller: a discrete-time tracking controller. There is no limitation on the type of control strategy to be used as long as the implementation constraints are met.
2. Generation code: a MATLAB code used to generate the designed controller, using the parameters and specifications listed in Subection 3.4. This code may use the provided Simulink model where the controller blocks are placed accordingly. The codes and models should be operative in MATLAB, version R2014a or newer.
3. Performance evaluation: results of the controller performance will be evaluated through the evaluation criteria indices defined in Subection 3.5. These values must be generated from a series of at least 20 simulations of each proposed controller to account for system uncertainties.
4. Sample comparison plots: four comparison plots of the four nominal cases simulated in the vRTHS tool. Both items 3 and 4 can be delivered in a pdf file.

A repository is available for all interested participants to contribute their codes and controllers to share with other RTHS researchers. These materials are available at <https://mechs.designsafe-ci.org/resources/>

5. Example implementation

445 In this section, a sample of a possible controller design for this benchmark problem is presented. Participants can use the steps provided in this sample to design, evaluate and verify their own controllers. Partitioning implications are discussed in Subsection 5.1, and the control design procedure is explained in Subsection 5.2. Subsection 5.3 presents an additional improvement of the controller by adding a phase-lead compensator. The RTHS results for both control approaches are included in Subsection 5.4.

450
455
460 Virtual RTHS simulations are executed for each one of the four partitioning choices defined in Subection 3.1. It is understood that proper performance and stability analysis has been made beforehand, to ensure an acceptable performance and a stable test. Although four verified partitioning choices are provided, if participants explore further cases, they should discuss the partitioning choices made and may perform a pre-test check similar to that made in Subsection 3.1, by any methodology of choice and only then, the next step of virtual simulation can be taken. As stated previously, the four cases provided herein have already been tested and represent a safe choice for performing initial simulations.

5.1. *Choice of partitioning*

465 Due to the broad base of users that are familiar with this method, we use PI control in this sample. A PI controller is chosen instead of a full proportional-integral-derivative (PID) to minimize noise amplification in the feedback loop [76]. This sample PI controller is designed with the following objectives 1) rise time of less than 0.05 sec; 2) overshoot less than 20%; and 3) settling time of at most 0.1 sec. These considerations are common practice for controllers that fall into the PID class. It should be mentioned that this tracking controller is implemented as an outer loop to the built-in servo controller normally found in transfer systems. The controller is designed (using the method of emulation) in continuous-time, and then the equations are converted into discrete-time. For purposes of visualization, the design procedure is explained using continuous-time variables.

470
475 The PI controller subsystem takes the form shown in Fig. 13 which is inside the tracking controller block in the block diagram of Fig. 7. Although the controller input for this particular sample is only the desired displacement of the first

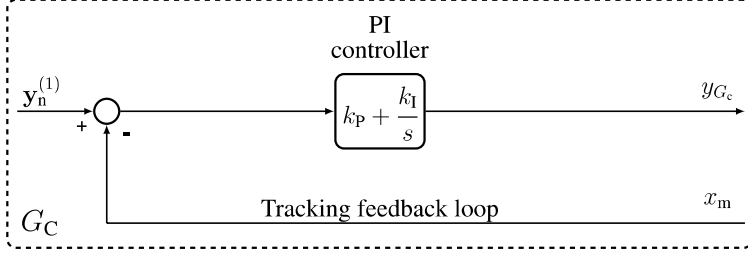


Figure 13: Block diagram of the PI controller.

floor, $y_n^{(1)}$, other available states and measurements may be used for different control methods. The proportional (k_p) and integral (k_i) gains of the PI controller shown in Fig. 13 can be manipulated accordingly to obtain the desired closed-loop dynamics of the system. The PI controller is tuned using the Ziegler-Nichols closed-loop method [77] and the gains, k_p and k_i that meet the predetermined goals are substituted in the controller expression, given by

$$G_C(s) = 2 + \frac{95}{s}. \quad (23)$$

The closed-loop frequency response of the compensated system and its comparison to the open-loop case is shown in Fig. 14 (open-loop and closed-loop shown in dotted and solid lines, respectively). Although the closed-loop system created with this controller is stable because the poles lie in the left half complex plane, the resulting time-delay shown in the bottom plot of Fig. 14 is of approximately 12 msec. If the designed controller does not meet the time-delay criteria stated in Subsection 3.4, the overall performance of the simulation, along with its stability may be seriously compromised. Therefore, this preliminary controller needs to be improved.

5.3. Time-delay compensation

As discussed in the previous section, the PI feedback controller alone is not sufficient to achieve acceptable performance in the vRTHS implementation. To address this concern, an additional component is included in the sample controller architecture. By observing the frequency response of the closed-loop system corresponding to the PI controller (Fig. 14, solid line), the phase margin criteria can be used to add a phase lead compensator to the PI controller to obtain an improved control plant response [76]. Phase-lead compensation is typically used to improve phase margin, which is the reason it is included in this particular control scheme. This compensator takes the form of a zero-pole combination, $G_T(s)$ in series with

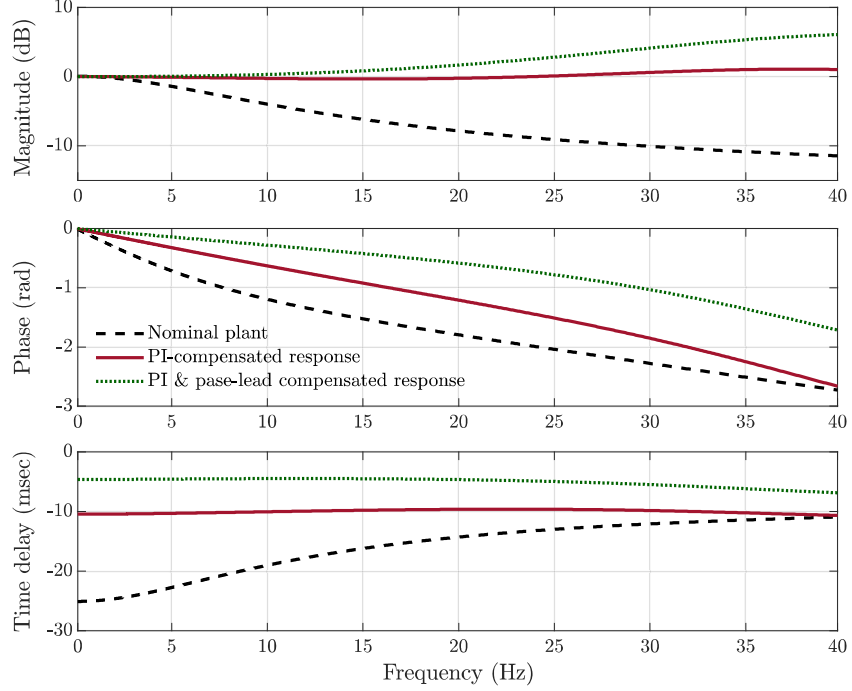


Figure 14: Frequency response comparison of the system with different levels of compensation.

the PI controller before the summing junction (Fig. 15) to avoid feedback noise amplification.

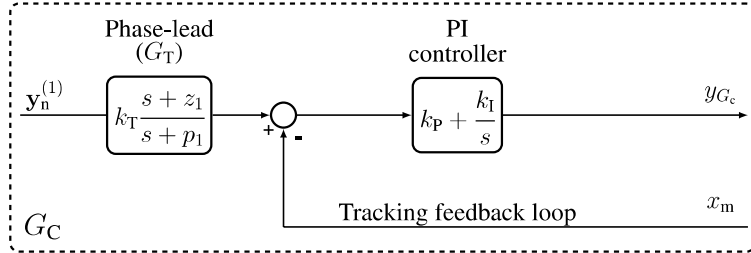


Figure 15: Block diagram of the PI controller with a phase lead compensator.

The phase lead compensator is mathematically expressed by the transfer function stated in the "Phase Lead" block of Fig. 15 with $z_1 < p_1$. Note that a zero near the imaginary plane and a pole far away from it are to be placed in such a way that the bandwidth of the closed-loop system increases producing a faster response. However, some unavoidable effects of this approach are an increase in the

high-frequency gain, which can amplify the high-frequency noise and produce a slight increase in the overshoot, yet achieving a better rise and settling times [76]. The phase lead compensator designed for this problem is given by

$$G_T = 50.8 \frac{s + 168.6}{s + 8570}. \quad (24)$$

- 505 Tustin's method is used to convert these continuous-time controllers into discrete-time representations [78]. The time-delay of the compensated system now reaches 5 msec, which meets the statement requirement.

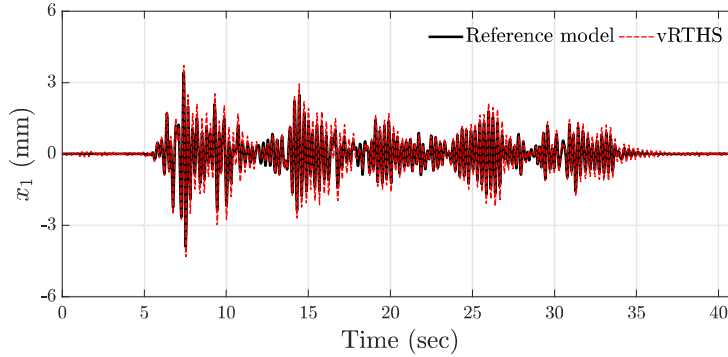
5.4. Virtual RTHS results with sample controller

The results of the virtual RTHS are presented in two parts: 1) the response comparison plots shown in Figs. 16 and 17; and, 2) the evaluation criteria values presented in Table 3. The improved time-delay obtained from the implementation of the phase-lead compensator is approximately 5.1 msec, which is less than the critical time-delay value for all four cases. When observing the response comparison plots of Fig. 16, good agreement is observed between the RTHS response and the reference model response for cases 1 and 2, where the damping/mass combination yields RTHS cases which are less sensitive to de-synchronization at the interface. This is also corroborated by the lower amounts of error observed in the evaluation criteria (Table 3).

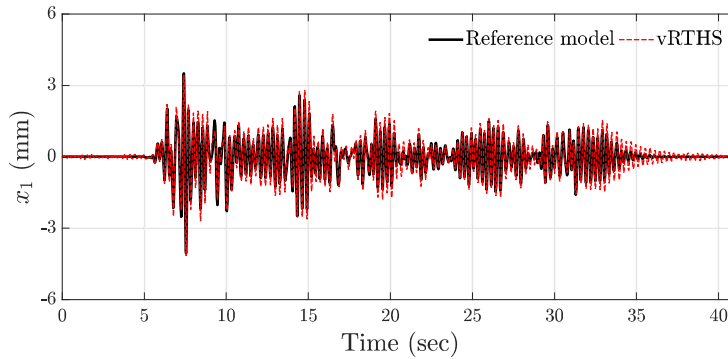
520 Similarly, the response comparison of cases 3 and 4 (Fig. 17) shows a higher difference between the vRTHS and reference responses. This is an indication that these two cases are more sensitive to de-synchronization at the interface, as predicted by the PSI analysis made previous to the tests, the error values also confirm this result. Also, note that the results are shown for the nominal controller. However, this controller is also stable in all four cases using 20 sets of random 525 parameters to confirm control robustness.

6. Closure

This paper presents a benchmark problem statement focused on RTHS for a seismically excited structure. Although the problem statement here considers the design of an effective transfer system tracking controller, the problem statement 530 and code package provide a framework that could be used to address additional research questions and more complex problems. The code package is available for download at <https://mechs.designsafe-ci.org>. A second phase of this benchmark problem is also envisioned. After this virtual simulation phase,



(a) Case 1



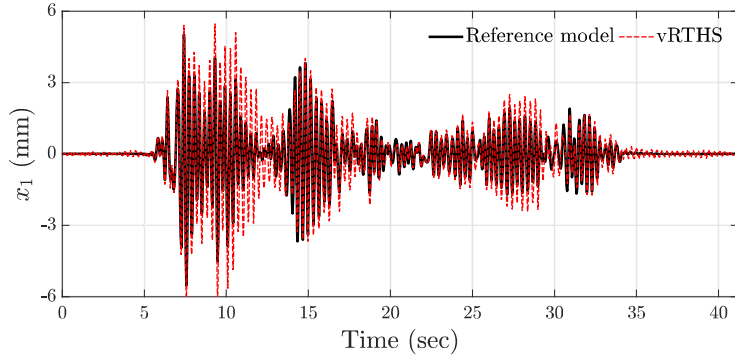
(b) Case 2

Figure 16: vRTHS response comparison of the 1st floor displacement under El Centro excitation, cases 1 and 2.

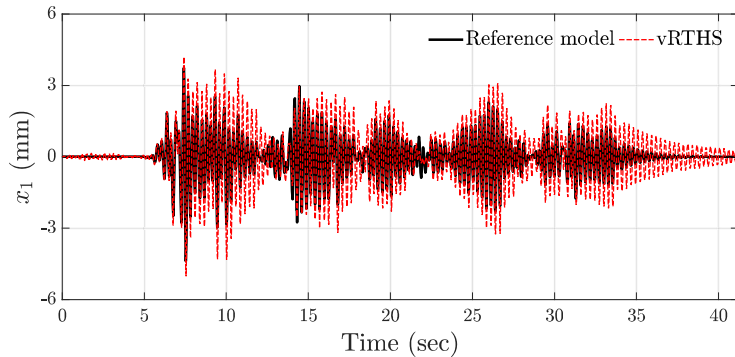
Case (#)	J_1 (msec)	J_2 (%)	J_3 (%)	J_4 (%)	J_5 (%)	J_6 (%)	J_7 (%)	J_8 (%)	J_9 (%)
1	4.6	10.4	11.5	36.1	19.0	32.3	32.4	14.8	14.8
2	4.6	9.8	11.1	33.1	17.1	30.5	30.5	15.3	15.2
3	4.6	9.1	10.2	49.9	36.7	49.8	49.8	35.5	35.6
4	4.6	10.5	11.3	72.6	35.2	68.5	68.7	33.4	33.3

Table 3: Virtual RTHS evaluation criteria for cases 1-4 for El Centro earthquake excitation, using a PI tracking controller improved with a phase lead compensator.

implementation and assessment of those controllers developed across the research



(a) Case 3



(b) Case 4

Figure 17: vRTHS response comparison of the 1st floor displacement under El Centro excitation, cases 3 and 4.

535 community can be explored on the physical setup at the IISL at Purdue University.

Acknowledgement

The authors would like to express their appreciation for the support from the Human Talent Promotion Institute (IFTH), of the Government of Ecuador, and the Colombia-Purdue Institute for Advanced Scientific Research (CPI) and Universidad del Valle, Cali-Colombia. The authors would also like to thank Johnny Condori from Purdue University, as well as Gaston Fernandois and Amirali Najaifi from the Smart Structures Technology Laboratory at the University of Illinois at Urbana-Champaign for their valuable feedback on this problem statement.
540

References

- 545 [1] M. Hakuno, M. Shidawara, T. Hara, Dynamic destructive test of a cantilever beam, controlled by an analog-computer, Proceedings of the Japan Society of Civil Engineers 1969 (171) (1969) 1–9. doi:10.2208/jscej1969.1969.171_1.
- 550 [2] K. Takanashi, K. Udagawa, M. Seki, T. Okada, H. Tanaka, Nonlinear earthquake response analysis of structures by a computer-actuator on-line system: Part I: detail of the system, Bulletin of Earthquake Resistant Structure Research Center 8 (1975) 1–17. doi:doi.org/10.3130/aijsaxx.229.0_77.
- 555 [3] K. Udagawa, K. Takanashi, H. Tanaka, Nonlinear earthquake response analysis of structures by a computer-actuator on-line system: Part II: response analyses of one bay-one story steel frames with inelastic beams, Transactions of the Architectural Institute of Japan 268 (0) (1978) 49–59. doi:10.3130/aijsaxx.268.0_49.
- 560 [4] K. Takanashi, K. Udagawa, H. Tanaka, Nonlinear earthquake response analysis of structures by a computer-actuator on-line system: Part III: reponse analyses of 1-bay 2-story steel frames, Transactions of the Architectural Institute of Japan 288 (0) (1980) 115–124. doi:10.3130/aijsaxx.288.0_115.
- 565 [5] K. Takanashi, K. Ohi, Earthquake response analysis of steel structures by rapid computer-actuator on-line system: Part I: a progress report, trial system and dynamic response of steel beams, Bull. Earthquake Resistant Struct. Research Center (ERS) - (16) (1983) 103–109.
- 570 [6] S. N. Dermitzakis, S. A. Mahin, Development of substructuring techniques for on-line computer controlled seismic performance testing, Ph.D. thesis, University of California, Berkeley (1985). doi:10.12681/eadd/4736.
- [7] M. Nakashima, H. Kato, E. Takaoka, Development of real-time pseudo dynamic testing, Earthquake Engineering & Structural Dynamics 21 (1) (1992) 79–92. doi:10.1002/eqe.4290210106.
- 575 [8] P. B. Shing, M. Nakashima, O. S. Bursi, Application of pseudodynamic test method to structural research, Earthquake Spectra 12 (1) (1996) 29–56. doi:10.1193/1.1585867.

- [9] J. Dimig, C. Shield, C. French, F. Bailey, A. Clark, Effective force testing: A method of seismic simulation for structural testing, *Journal of Structural Engineering* 125 (9) (1999) 1028–1037. doi:10.1061/(asce)0733-9445(1999)125:9(1028).
- [10] M. S. Williams, A. Blakeborough, Laboratory testing of structures under dynamic loads: an introductory review, *Philosophical Transactions of the Royal Society A: Mathematical, Physical and Engineering Sciences* 359 (1786) (2001) 1651–1669. doi:10.1098/rsta.2001.0860.
- [11] M. Nakashima, Development, potential, and limitations of real-time online (pseudo-dynamic) testing, *Philosophical Transactions of the Royal Society of London A: Mathematical, Physical and Engineering Sciences* 359 (1786) (2001) 1851–1867. doi:10.1098/rsta.2001.0876.
- [12] O. Kwon, V. Kammula, Model updating method for substructure pseudo-dynamic hybrid simulation, *Earthquake Engineering & Structural Dynamics* 42 (13) (2013) 1971–1984. doi:10.1002/eqe.2307.
- [13] H. N. Mahmoud, A. S. Elnashai, B. F. Spencer Jr., O.-S. Kwon, D. J. Bennier, Hybrid simulation for earthquake response of semirigid partial-strength steel frames, *Journal of structural engineering* 139 (7) (2013) 1134–1148. doi:doi.org/10.1061/(asce)st.1943-541x.0000721.
- [14] G. Abbiati, O. S. Bursi, P. Caperan, L. Di Sarno, F. J. Molina, F. Paolacci, P. Pegon, Hybrid simulation of a multi-span RC viaduct with plain bars and sliding bearings, *Earthquake Engineering & Structural Dynamics* 44 (13) (2015) 2221–2240. doi:10.1002/eqe.2580.
- [15] D. Gomez, S. J. Dyke, A. Maghareh, Enabling role of hybrid simulation across NEES in advancing earthquake engineering, *Smart Structures and Systems* 15 (3) (2015) 913–929. doi:10.12989/sss.2015.15.3.913.
- [16] P. B. Shing, S. A. Mahin, Computational aspects of a seismic performance test method using on-line computer control, *Earthquake Engineering & Structural Dynamics* 13 (4) (1985) 507–526. doi:doi.org/10.1002/eqe.4290130406.

- [17] S. A. Mahin, P. shum B. Shing, Pseudodynamic method for seismic testing, *Journal of Structural Engineering* 111 (7) (1985) 1482–1503. doi:10.1061/(asce)0733-9445(1985)111:7(1482).
- [18] N. Castaneda, X. Gao, S. J. Dyke, Computational tool for real-time hybrid simulation of seismically excited steel frame structures, *Journal of Computing in Civil Engineering* 29 (3) (2013) 04014049. doi:10.1061/(asce)cp.1943-5487.0000341.
- [19] E. Watanabe, T. Kitada, S. Kunitomo, K. Nagata, Parallel pseudodynamic seismic loading test on elevated bridge system through the internet, in: The Eight East Asia-Pacific Conference on Structural Engineering and Construction, 2001, pp. –.
- [20] G. Mosqueda, Continuous hybrid simulation with geographically distributed substructures, Ph.D. thesis, University of California at Berkeley (2003).
- [21] B. F. Spencer Jr., A. Elnashai, N. Nakata, H. Saliem, G. Yang, J. Futrelle, ..., P. Stauffer, The MOST experiment: earthquake engineering on the grid. workshop on case studies on grid applications, Technical Report, NEEgrid.
- [22] O. Kwon, N. Nakata, A. Elnashai, B. F. Spencer Jr., Technical note. a framework for multi-site distributed simulation and application to complex structural systems, *Journal of Earthquake Engineering* 9 (5) (2005) 741–753. doi:10.1080/13632460509350564.
- [23] S. J. Kim, R. E. Christenson, B. M. Phillips, B. F. Spencer Jr., Geographically distributed real-time hybrid simulation of mr dampers for seismic hazard mitigation, in: 20th Analysis and Computation Specialty Conference, 2012, pp. 382–393. doi:10.1061/9780784412374.034.
- [24] A. I. Ozdagli, Distributed real-time hybrid simulation: Modeling, development and experimental validation, Ph.D. thesis, Purdue University (2015).
- [25] J. E. Carrion, B. F. Spencer Jr., Model-based strategies for real-time hybrid testing, Tech. rep., Newmark Structural Engineering Laboratory. University of Illinois at Urbana-Champaign. (2007).
- [26] R. E. Christenson, Y. Z. Lin, A. Emmons, B. Bass, Large-scale experimental verification of semiactive control through real-time hybrid simulation, *Journal of Structural Engineering* 134 (4) (2008) 522–534. doi:10.1061/(ASCE)0733-9445(2008)134:4(522).

- [27] B. M. Phillips, S. Takada, B. F. Spencer Jr., Y. Fujino, Feedforward actuator controller development using the backward-difference method for real-time hybrid simulation, *Smart Structures and Systems* 14 (6) (2014) 1081–1103. doi:10.12989/sss.2014.14.6.1081.
- 645 [28] O. Mercan, J. M. Ricles, Experimental Studies on Real-Time Testing of Structures with Elastomeric Dampers, *Journal of Structural Engineering* 135 (9) (2009) 1124–1133. doi:10.1061/(ASCE)0733-9445(2009)135:9(1124).
- 650 [29] C. Chen, J. M. Ricles, T. L. Karavasilis, Y. Chae, R. Sause, Evaluation of a real-time hybrid simulation system for performance evaluation of structures with rate dependent devices subjected to seismic loading, *Engineering Structures* 35 (2012) 71–82. doi:10.1016/j.engstruct.2011.10.006.
- 655 [30] N. Nakata, M. Stehman, Compensation techniques for experimental errors in real-time hybrid simulation using shake tables, *Smart Structures and Systems* 14 (6) (2014) 1055–1079. doi:10.12989/sss.2014.14.6.1055.
- 660 [31] Y. J. Cha, A. Agrawal, A. Friedman, B. Phillips, R. Ahn, B. Dong, S. J. Dyke, B. F. Spencer Jr., J. Ricles, R. E. Christenson, Performance validations of semiactive controllers on large-scale moment-resisting frame equipped with 200-kN MR damper using real-time hybrid simulations, *Journal of Structural Engineering* 140 (10) (2014) 04014066. doi:10.1061/(ASCE)ST.1943-541X.0000982.
- 665 [32] K. M. Mosalam, S. Günay, Seismic performance evaluation of high voltage disconnect switches using real-time hybrid simulation: I. System development and validation, *Earthquake Engineering & Structural Dynamics* 43 (8) (2014) 1205–1222. doi:10.1002/eqe.2395.
URL <http://doi.wiley.com/10.1002/eqe.2395>
- 670 [33] G. A. Fernandois, B. F. Spencer Jr., Model-based framework for multi-axial real-time hybrid simulation testing, *Earthquake Engineering and Engineering Vibration* 16 (4) (2017) 671–691. doi:10.1007/s11803-017-0407-8.
- [34] M. Nakashima, N. Masaoka, Real-time on-line test for MDOF systems, *Earthquake engineering & structural dynamics* 28 (4) (1999) 393–420.

- 675 [35] J. E. Carrion, B. F. Spencer Jr., B. M. Phillips, Real-time hybrid simulation for structural control performance assessment, *Earthquake Engineering and Engineering Vibration* 8 (4) (2009) 481–492. doi:10.1007/s11803-009-9122-4.
- 680 [36] B. M. Phillips, B. F. Spencer Jr., Model-based framework for real-time dynamic structural performance evaluation, Tech. rep., Newmark Structural Engineering Laboratory, University of Illinois at Urbana-Champaign. (2012).
- 685 [37] G. Ou, A. I. Ozdagli, S. J. Dyke, B. Wu, Robust integrated actuator control: experimental verification and real-time hybrid-simulation implementation, *Earthquake Engineering & Structural Dynamics* 44 (3) (2015) 441–460. doi:10.1002/eqe.2479.
- [38] R. E. Christenson, Advances in real-time hybrid simulation, Tech. rep., University of Lehigh (Dec 2011).
- 690 [39] S. J. Dyke, N. Nakata, M. Gmez, Report on the discussions during the hybrid simulation workshop, Tech. rep., Purdue University (Aug 2015).
- [40] A. Pinto, R. E. Christenson, S. J. Dyke, Advances in real-time hybrid simulation, Tech. rep., United States (US) – European Union (EU) Workshop on Real-Time Hybrid Simulation (Dec 2015).
- 695 [41] C. Whyte, G. Abbiati, S. Bozidar, State-of-the-art and future directions of hybrid modeling and simulation, Tech. rep., ETH, Swiss Federal Institute of Technology, Zurich (May 2016).
- [42] MECHS, 1st multihazard engineering collaboratory on hybrid simulation research coordination network. Breaking barriers and building capacity (2018).
- 700 [43] N. Nakata, S. J. Dyke, J. Zhang, G. Mosqueda, X. Shao, H. Mahmoud, . . . , C. Song, Hybrid simulation primer and dictionary (2014).
- [44] B. F. Spencer Jr., R. E. Christenson, S. J. Dyke, Next generation benchmark control problem for seismically excited buildings, in: Proceedings of the Second World Conference on Structural Control, Vol. 2, Kyoto Japan, 1998, pp. 1135–1360.

- [45] B. F. Spencer Jr., S. J. Dyke, H. S. Deoskar, Benchmark problems in structural control: part II—active tendon system, *Earthquake engineering & structural dynamics* 27 (11) (1998) 1141–1147. doi:10.1002/(SICI)1096-9845(1998110)27:11\%3C1141::AID-EQE775\%3E3.0.CO;2-S.
- [46] B. F. Spencer Jr., S. J. Dyke, H. S. Deoskar, Benchmark problems in structural control: Part I—active mass driver system, *Earthquake Engineering & Structural Dynamics* 27 (11) (1998) 1127–1139. doi:10.1002/(SICI)1096-9845(1998110)27:11\%3C1127::AID-EQE774\%3E3.0.CO;2-F.
- [47] S. J. Dyke, D. Bernal, J. L. Beck, C. Ventura, An experimental benchmark problem in structural health monitoring, in: *Proceedings of the 3rd International Workshop on Structural Health Monitoring*, CRC Press, 2001, pp. 488–497.
- [48] D. Bernal, S. J. Dyke, H. F. Lam, J. L. Beck, Phase II of the ASCE benchmark study on SHM, in: *Proceedings of the 15th ASCE engineering mechanics conference*, Columbia University, 2002, pp. –.
- [49] S. J. Dyke, D. Bernal, J. Beck, C. Ventura, Experimental phase II of the structural health monitoring benchmark problem, in: *Proceedings of the 16th ASCE engineering mechanics conference*, 2003, pp. –.
- [50] S. J. Dyke, J. M. Caicedo, G. Turan, L. A. Bergman, S. Hague, Phase I benchmark control problem for seismic response of cable-stayed bridges, *Journal of Structural Engineering* 129 (7) (2003) 857–872. doi:10.1061/(ASCE)0733-9445(2003)129:7(857).
- [51] J. M. Caicedo, S. J. Dyke, S. J. Moon, L. A. Bergman, G. Turan, S. Hague, Phase II benchmark control problem for seismic response of cable-stayed bridges, *Journal of Structural Control* 10 (3-4) (2003) 137–168. doi:10.1002/stc.23.
- [52] Y. Ohtori, R. E. Christenson, B. F. Spencer Jr., S. J. Dyke, Benchmark control problems for seismically excited nonlinear buildings, *Journal of Engineering Mechanics* 130 (4) (2004) 366–385. doi:10.1061/(ASCE)0733-9399(2004)130:4(366).

- [53] J. N. Yang, A. Agrawal, B. Samali, J.-C. Wu, Benchmark problem for response control of wind-excited tall buildings, *Journal of Engineering Mechanics* 130 (4) (2004) 437–446. doi:10.1061/(ASCE)0733-9399(2004)130:4(437).
- [54] E. A. Johnson, H. F. Lam, L. S. Katafygiotis, J. L. Beck, Phase I IASC-ASCE structural health monitoring benchmark problem using simulated data, *Journal of engineering mechanics* 130 (1) (2004) 3–15. doi:10.1061/(ASCE)0733-9399(2004)130:1(3).
- [55] S. Narasimhan, S. Nagarajaiah, E. A. Johnson, H. P. Gavin, Smart base-isolated benchmark building. part I: problem definition, *Structural Control and Health Monitoring: The Official Journal of the International Association for Structural Control and Monitoring and of the European Association for the Control of Structures* 13 (2-3) (2006) 573–588. doi:10.1002/stc.99.
- [56] S. Narasimhan, S. Nagarajaiah, E. A. Johnson, Smart base-isolated benchmark building part IV: Phase II sample controllers for nonlinear isolation systems, *Structural Control and Health Monitoring: The Official Journal of the International Association for Structural Control and Monitoring and of the European Association for the Control of Structures* 15 (5) (2008) 657–672. doi:10.1002/stc.267.
- [57] A. Agrawal, P. Tan, S. Nagarajaiah, J. Zhang, Benchmark structural control problem for a seismically excited highway bridge—part I: Phase I problem definition, *Structural Control and Health Monitoring: The Official Journal of the International Association for Structural Control and Monitoring and of the European Association for the Control of Structures* 16 (5) (2009) 509–529. doi:10.1002/stc.301.
- [58] S. J. Dyke, Report on the building structural health monitoring problem phase 1 experimental (Jan 2011).
URL <https://datacenterhub.org/resources/2808>
- [59] S. J. Dyke, Report on the building structural health monitoring problem phase 2 analytical (Jan 2011).
URL <https://datacenterhub.org/resources/2810>
- [60] MATLAB, version 8.3 (R2014a), The MathWorks Inc., Natick, Massachusetts, 2014.

- [61] X. Gao, Development of a robust framework for real-time hybrid simulation: From dynamical system, motion control to experimental error verification, Ph.D. thesis, Purdue University (2012).
- 775 [62] X. Gao, N. Castaneda, S. J. Dyke, Experimental validation of a generalized procedure for MDOF real-time hybrid simulation, *Journal of Engineering Mechanics* 140 (4) (2013) 04013006.
- 780 [63] X. Gao, N. Castaneda, S. J. Dyke, Real time hybrid simulation: From dynamic system, motion control to experimental error, *Earthquake Engineering and Structural Dynamics* 42 (6) (2013) 815–832. doi:10.1002/eqe.2246.
- [64] A. K. Chopra, et al., *Dynamics of structures*, Vol. 3, Prentice Hall New Jersey, 1995.
- 785 [65] R. M. Botelho, R. E. Christenson, Robust stability and performance analysis for multi-actuator real-time hybrid substructuring, in: *Dynamics of Coupled Structures*, Volume 4, Springer, 2015, pp. 1–7. doi:10.1007/978-3-319-15209-7_1.
- 790 [66] O. Mercan, J. M. Ricles, Stability analysis for real-time pseudodynamic and hybrid pseudodynamic testing with multiple sources of delay, *Earthquake Engineering & Structural Dynamics* 37 (10) (2008) 1269–1293. doi:10.1002/eqe.814.
- [67] A. Maghareh, S. J. Dyke, A. Prakash, J. F. Rhoads, Establishing a stability switch criterion for effective implementation of real-time hybrid simulation, *Smart Structures and Systems* 14 (6) (2014) 1221–1245. doi:10.12989/ssss.2014.14.6.1221.
- 795 [68] A. Maghareh, S. J. Dyke, S. Rabieniaharatbar, A. Prakash, Predictive stability indicator: A novel approach to configuring a real-time hybrid simulation, *Earthquake Engineering & Structural Dynamics* 46 (1) (2017) 95–116. doi:10.1002/eqe.2775.
- 800 [69] T. Horiuchi, T. Konno, Development of a real-time hybrid experimental system with actuator delay compensation (1st report compensation method and application to experiments of single-degree-of-freedom systems), *Transactions of the Japan Society of Mechanical Engineers, Series C* 61 (584) (1995) 1328–1336.

- 805 [70] Y. Chae, K. Kazemibidokhti, J. M. Ricles, Adaptive time series compensator
for delay compensation of servo-hydraulic actuator systems for real-time
hybrid simulation, *Earthquake Engineering & Structural Dynamics* 42 (11)
(2013) 1697–1715. doi:10.1002/eqe.2294.
- 810 [71] R. E. Christenson, S. J. Dyke, J. Zhang, G. Mosqueda, C. Chen, N. Nakata,
P. Laplace, W. Song, Y. Chae, G. Marshall, G. Ou, C. A. Riascos, C. Song,
Hybrid simulation: A discussion of current assessment measures, Purdue
University.
- 815 [72] F. Lin, A. Maghreh, S. J. Dyke, X. Lu, Experimental implementation of
predictive indicators for configuring a real-time hybrid simulation, *Engineering
Structures* 101 (2015) 427–438. doi:doi.org/10.1016/j.
engstruct.2015.07.040.
- 820 [73] A. Maghreh, C. E. Silva, S. J. Dyke, Servo-hydraulic actuator in control-
lable canonical form: Identification and experimental validation, *Mechanical
Systems and Signal Processing* 100 (2018) 398–414. doi:10.1016/j.
ymssp.2017.07.022.
- 825 [74] S. J. Dyke, B. F. Spencer Jr., P. Quast, M. K. Sain, Role of control-structure
interaction in protective system design, *Journal of Engineering Mechanics*
121 (2) (1995) 322–338. doi:10.1061/(asce)0733-9399(1995)
121:2 (322).
- [75] D. H. Kim, T. C. Tsao, A linearized electrohydraulic servovalve model
for valve dynamics sensitivity analysis and control system design, *Journal
of Dynamic Systems, Measurement, and Control* 122 (1) (2000) 179–187.
doi:10.1115/1.482440.
- 830 [76] B. C. Kuo, *Automatic control systems*, Prentice Hall PTR, 1987.
- [77] J. G. Ziegler, N. B. Nichols, Optimum settings for automatic controllers,
trans. ASME 64 (11). doi:10.1115/1.2899060.
- 835 [78] Y. Koren, *Computer control of manufacturing systems*, Vol. 98, McGraw-
Hill New York et al., 1983.